Design, Fabrication and Characterization of PVA/Nanocarbon Composite Fibers

by

Rahul Verma

A Thesis Presented in Partial Fulfillment
of the Requirements for the Degree
Master of Science

Approved November 2018 by the
Graduate Supervisory Committee:

Kenan Song, Chair
Hanqing Jiang
Qiong Nian

ARIZONA STATE UNIVERSITY

December 2018

ABSTRACT

Polymer fibers have broad applications in wearable electronics, bulletproof vests, batteries, fuel cells, filters, electrodes, conductive wires, and biomedical materials. Polymer fibers display light density and flexibility but are mostly weak and compliant. The ceramic, metallic, and carbon nanoparticles have been frequently included in polymers for fabricating continuous, durable, and functional composite fibers. Nanoparticles display large specific areas, low defect density and can transfer their superior properties to polymer matrices. The main focus of this thesis is to design, fabricate and characterize the polymer/nanocarbon composite fibers with unique microstructures and improved mechanical/thermal performance. The dispersions and morphologies of graphene nanoplatelets (GNPs), the interactions with polyvinyl alcohol (PVA) molecules and their influences on fiber properties are studied. The fibers were fabricated using a dry-jet wet spinning method with engineered spinneret design. Three different structured fibers were fabricated, namely, one-phase polymer fiber (1-phase), two-phase core-shell composite fiber (2-phase), and three-phase co-axial composite fiber (3-phase). These polymer or composite fibers were processed at three stages with drawing temperatures of 100˚C, 150˚C, and 200˚C. Different techniques including the mechanical tester, wide-angle X-Ray diffraction (WAXD), scanning electron microscope (SEM), thermogravimetric analysis (TGA), and differential scanning calorimeter (DSC) have been used to characterize the fiber microstructures and properties.

This thesis is dedicated to my parents, family and friends who have been my pillar of emotional support, a beacon of light and persistently reminded me of my goals in life and the success I have worked towards.

TABLE OF CONTENTS

LIST OF TABLES

LIST OF FIGURES

LIST OF SYMBOLS AND ABBREVIATIONS

Materials	
CATB	Cetyltrimethylammonium bromide
CNM	Carbon nanomaterial
CNT	Carbon nanotube
DMSO	Dimethyl sulphoxide
EPD	Ethylene propylene diene
EVA	Ethylene-co-vinyl acetate
GF	Graphite flakes
GNP	Graphene nanoplatelets
GO	Graphite oxide
NMP	N-methyl-2-pyrrolidone
PA	Polyamides
PAN	Polyacrylonitrile
PE	Polyethylene
PET	Poly-ethylene terephthalate
PP	Polypropylene
PVA	Polyvinyl alcohol
PST	Polystyrene
RGO	Reduced graphene oxide
SDBS	Sodium dodecyl benzene sulfonate
SDS	Sodium dodecyl sulfate
Characterizations	
DSC	Differential scanning calorimetry
SEM	Scanning electron microscope
TGA	Thermogravimetric analysis
WAXD	Wide angle x-ray diffraction

CHAPTER 1 INTRODUCTION
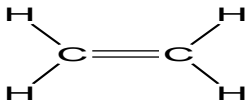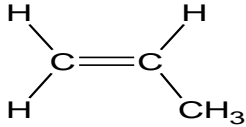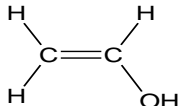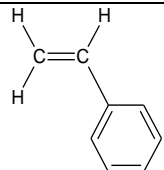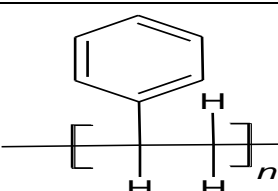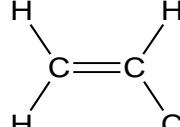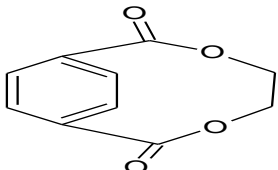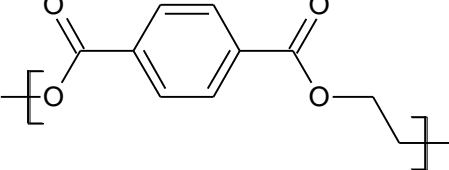
1.1   Polymer-based nanoparticle-included composites

Polymer nanocomposites are composed of two or more phases with the polymer as matrix and nanoparticles as reinforcement fillers. Nanoparticles are materials with sizes ranging from one nanometer to a few hundred nanometers.

1.1.1   Polymers

Polymers include natural polymers and synthesized polymers. Natural polymers such as cellulose, lignin, silk, wool, and latex, have long existed and play ubiquitous roles in everyday life. In 1869, the first semi-synthetic polymer was invented by John Wesley Hyatt. He treated cellulose derived from cotton fiber and discovered a synthetic plastic that could take a variety of shapes and imitate natural materials. Synthesized polymers did not appear until the 1900s. In 1907, the first fully synthetic polymer, Bakelite, invented by Leo Bakeland was found to be mechanically durable, thermally insulated, and shape mouldable. In 1935, Wallace Hume Carothers produced the first commercially successful synthetic thermoplastic polymer, nylon, at the DuPont's research facility. The nylon was melt-processed into fibers, films or other complex shapes. The invention of Bakelite and nylon, as well as other macromolecules, inspired the study of polymer science, which differentiated the molecules from previously known metals, ceramics, and small molecules. The development of polymer science, including the understanding of polymeric chain structure as macromolecules with definite molecular weight, expanded the syntheses of polymer families to neoprene and polyester.

Table 1 Some common types of polymers

Some common types of polymers		
Example	**Monomer**	**Polymer**
Polyethylene		$\left[CH_2-CH_2 \right]_n$
Polypropylene		
Polyvinyl Alcohol		
Polystyrene		
Polyvinyl Chloride		
Polyethylene Terephthalate		

Polymers are macromolecules made of many repeat units (i.e., monomers) within the chained structure (Table 1). The repeating number of monomers, termed as the degree of polymerization (DP), ranges from thousands to hundreds of thousands and defines the polymer molecular weight (M_w) (Table 1). Larger values of molecular weight generally correspond to longer polymer chain length, higher entanglement density, and, better

mechanical toughness, thermal stability, and chemical resistance. Polymers based on their intra-molecular bonding types can be classified as thermoplastics and thermosets. For thermoplastics, the bonding among polymer chains is secondary van der Waals forces while for thermosets, the linkages are chemical linkages (figure 1). General thermoplastics include polypropylene (PP), polyethylene (PE), poly (ethylene-co-vinyl acetate) (EVA), poly (ethylene propylene diene) rubber (EPDM), polyamides (PA), polyethylene terephthalate (PET), and polystyrene (PS). General thermosets are bakelite, epoxy resin, and polyurethane elastomers.[1]
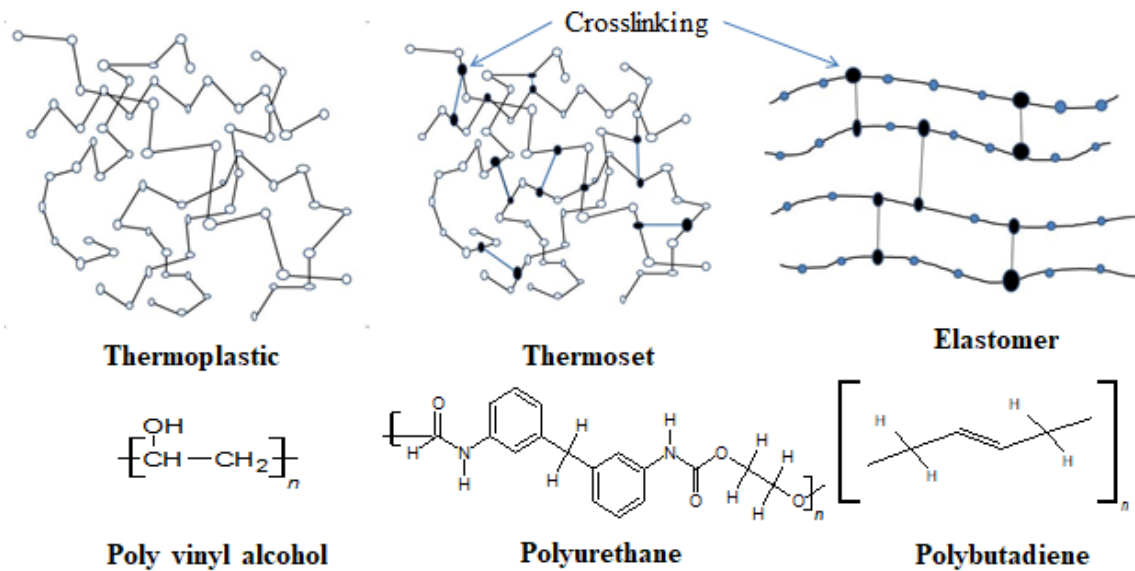
Figure 1 Thermosets, thermoplastics, and elastomers

1.1.2 Nanoparticles

Nanoparticles are fillers that have at least one dimension, at a length scale of nanometers, and three dimension numbers that describe the size and shape of such particles. In practice, many anisometric particles may be considered as rotational symmetric, for example, disks and rods. In this case, only two dimension numbers are necessary for a

description of size and shape, i.e., the sizes are the extension in the direction of the rotational axis and the maximum extension in the direction perpendicular to it, namely, an equivalent diameter and an aspect ratio. Based on their morphology, nanoparticles can be categorized into zero-dimensional (0D), one-dimensional (1D), and two-dimensional (2D), including 0D quantum dots, 1D nanowires and 2D sheets (Figure 2). [2]
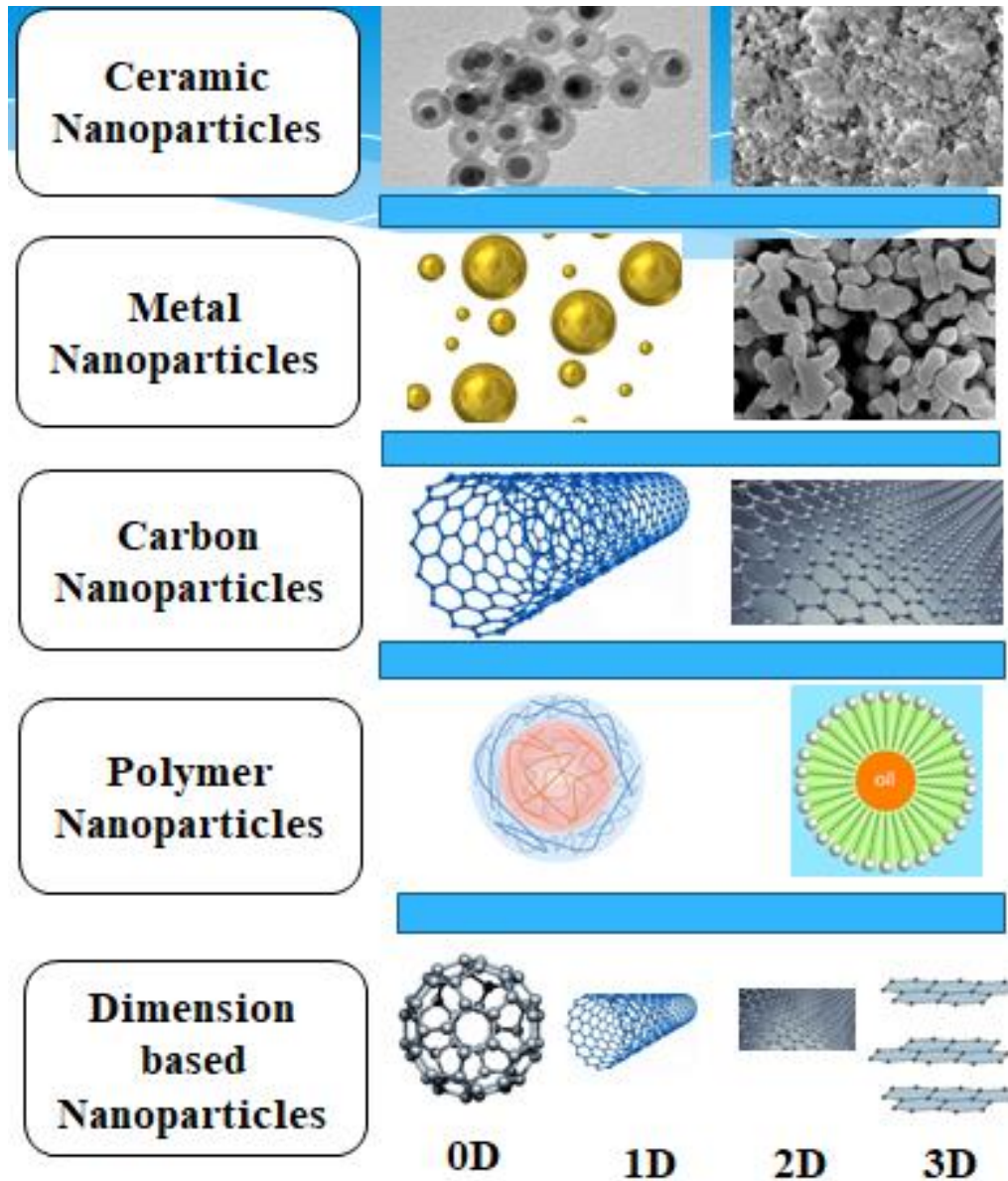
Figure 2 Different categories of nanofillers

Nanoparticles can also be categorized based on the material compositions, which includes ceramic, metal, semiconductor, carbon, and polymer nanoparticles (Figure 2). Ceramic nanoparticles are inorganic solids made up of oxides, carbides, carbonates, and phosphates. They have high heat resistance and chemical inertness for photo-degradation of dyes, drug delivery, and imaging. Metal nanoparticles are prepared from metal precursors and can be synthesized by chemical, electrochemical, or photochemical methods. In chemical methods, the metal nanoparticles are obtained by reducing the metal ion precursors in solution by chemical reducing agents. Their considerable surface energy and capabilities to adsorb small molecules can be used for detection, imaging of biomolecules, and, in environmental and bioanalytical applications. Semiconductor nanoparticles have properties like metals and nonmetals. These particles have very wide bandgaps and are used in photocatalysis, electronics devices, photo optics, and water splitting applications. Some examples are GaN, GaP, InP, ZnO, ZnS, CdS, CdSe, and CdTe. Polymeric nanoparticles are organic based nanoparticles. Depending on the methods of preparations, they have structured shapes such as nanocapsules or nanospheres, with potential applications in drug delivery and diagnostics. Carbon nanoparticles include fullerene, carbon nanotubes and graphene, which can be used in structural, thermal and electrical applications.

1.1.3 Key factors in the polymer/nanoparticle composite structural control

In nanocomposites, different components exist, and there is a contrast in their composition, interaction, and properties. Several key factors affect the role nanoparticles play as reinforcing fillers in a polymer matrix, including:

(a) Nanoparticle dispersions: The nanoparticle dispersion procedure involves sonication in a bath, with a tip, at the absence or presence of surfactants for a period. The mechanical energy generated during sonication overcomes the van der Waals forces between nanoparticles leading to exfoliation of the fillers. Surfactants are commonly used to disperse nanoparticles in solvents. Typical surfactants include sodium dodecyl benzenesulfonate (SDBS), sodium dodecyl sulfate (SDS), cetyltrimethylammonium bromide (CATB), sodium *n*-lauroyl sarcosinate, and nonylphenol ethoxylate. For example, graphene can be dispersed in water with the aid of surfactants such as SDS, SDBS, CATB, and tetradecyl trimethyl ammonium bromide. Organic solvents such as DMF, NMP (N-Methyl-2-pyrrolidone), and cyclohexanone have successfully exfoliated graphene.

(b) Polymer/nanoparticle interfacial interactions: The interface between the filler particles and the matrix in a polymer nanocomposite constitutes a much higher area within the bulk material as compared to conventional composites, and hence, influences the composite properties to a much greater extent, even at a low filler loading. There are three main material constituents in any composite: the matrix, the reinforcement, and the interfacial region. The interfacial area is responsible for 'communication' between the matrix and filler and is conventionally ascribed properties different from the bulk matrix because of its proximity to the surface of the filler. The interfacial strength between filler and polymer is an important factor in making filler/polymer nanocomposites. The lack of adhesion between the filler and polymer can cause the formation of strongly bonded nanoparticles aggregates during the nanocomposite preparation or can result in an early failure at the interface, and thus, changes the physical properties of the final composite.

To increase interaction between the polymer and the filler, polymers can be grafted to nanoparticles. There are two methods: the first, commonly referred to as the "grafting to" approach, involves preformed polymer chains reacting with the surface of nanoparticles. The second method, referred to as the "grafting from" approach, involves the polymerization of monomers on nanotube surfaces.

(c) Nanoparticle orientations: Nanoparticle alignment generally can be achieved through fabrication methods, such as spinning techniques (e.g., dry-jet wet spinning and subsequent annealing and drawing of fibers). Other methods, such as electrical field, magnetic field, and sonic-based methods, are also used (Table 2). Oriented nanoparticles along polymer chains facilitate the anisotropic properties in nanocomposites.

Table 2 Nanoparticle orientation in ex-situ field

External fields	Description	References
Mechanical/drawing	A heat-stress coupled technique to induce strong molecular orientation and thereby crystallization in crystalline polymers.	2018[3], 2014[4], 2016[5], 2005[6]
Electrical	When subjected to an external electric field, the particulate particles are polarized, generating electric dipoles. The interaction of opposite dipoles results in the chaining of particles	2018[3], 2015[7], 2009[8], 2012[9]
Magnetic	Nanoparticles are oriented parallel to the magnetic fields when their suspension in organic solvents are placed in a magnetic field	2018[3], 2018[10], 2018[11], 2007[12]

1.2   Fiber spinning review

Fiber spinning is the process of extruding polymer solutions or melts from the spinneret and forming continuous fibers. The polymer solutions or melts are referred to as 'dope" or "spinning dope". Spinneret extrusion methods can be classified as according to the

7

nature of the spinning dope, namely, melt spinning, dry spinning, wet spinning, gel spinning, electrospinning, and solution blow spinning (Figure 3).
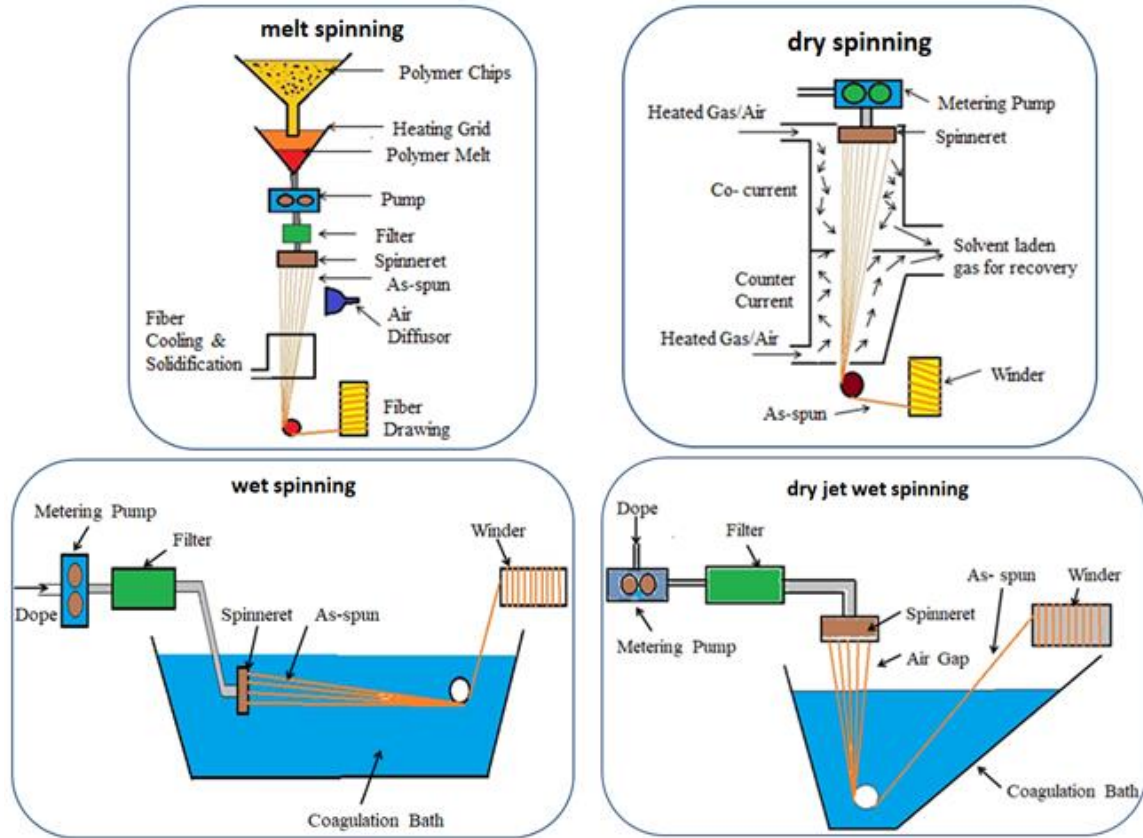
Figure 3 Different types of spinning techniques (a) melt spinning (b) dry spinning (c) wet spinning (d) dry-jet wet spinning

Table 3 listed all processes and features of these spinnings methods, among which dry-jet wet spinning can spin thin diameter high-performance fibers and has been used in this research. As compared to dry spinning or wet spinning, dry-jet wet spinning combines the advantages of injecting fibers into the air for initial polymer chain alignment, low viscosity processing, and coagulating polymer solutions into gels for high draw ratios.

8

Table 3 Features of all spinning methods

Spinning Method	Processes	Features
Melt spinning[13,14,15]	The polymer granules are melted and extruded through the spinneret, and a metering pump controls the flow of molten liquid and the air to quench the fibers.	No solvent usage; requirement of energy-consuming and highly maintained instruments;
Dry spinning[16,17,18]	Polymer melts or solutions are injected into a heating chamber full of hot air or inert gas to solidify the fibers.	Fast solidification via solvent evaporations, flexible fiber shape controls; flammable solvent hazard, slow process;
Wet spinning[19,20,15]	The spinneret is immersed into a coagulation bath in which the polymer solution is extruded into a nonsolvent, leading to solvent removal from the fiber jet and solidification of the fiber as precipitation occurs.	Low viscosity, high collection speed; use of coagulants, slow diffusion processes;
Dry-jet wet spinning[21,22,23]	The polymer gels are injected into the air for drying and liquid bath for gelation and cooling.	Low viscosity, high draw ratios; massive consumption of coagulants, slow diffusion processes;
Electrospinning[24,25,26]	Use of an electric potential to overcome the surface tension of a solution to produce an ultra-fine jet which elongates, slenders, and solidifies as it travels through the electric field to a collector.	High-resolution nanoscale fibers, low defects in fibers; non-uniform feed rate, lack of continuous fiber collection, use of highly toxic chlorinated or fluorinated solvents;
Solution blow spinning[27,28,29]	Two parallel concentric fluid streams, i.e., a polymer dissolved in a volatile solvent and a pressurized gas that flows around the polymer solution are blown into fibers that are deposited in the direction of the gas flow.	deposit capability on both planar and nonplanar substrates cost efficiency; non-uniform fiber sizes, lack of continuous fiber collection.

1.3   Nanocomposite fibers

While there so many kinds of polymer-based nanoparticle-included composite fibers, this work will focus on polyvinyl alcohol (PVA)/graphene nanocomposite fibers.

1.3.1   PVA

Poly(vinyl alcohol) (PVA) is a water-soluble, biodegradable, synthetic polymer, and its degradability is enhanced through hydrolysis because of the presence of hydroxyl groups. PVA can be dissolved in water or DMSO, which require the solvent temperature to be ~ 100˚C with a holding time of 30 minutes. The properties of polyvinyl acetate depend on the extent or degree of hydrolysis, specifically whether it's full or partial. It influences its categorization into two types: partially hydrolyzed and fully hydrolyzed. PVA has a melting point of 230 °C and 170–190 °C for the fully hydrolysed and partially hydrolysed grades, respectively. It decomposes rapidly above 200 °C as it can undergo pyrolysis at high temperatures. The molecular weight for PVA products may vary from 10,000 – 50,000 depending on the length of the initial vinyl acetate polymer, the level of hydrolysis to eliminate the acetate groups and whether it occurs in acidic or alkaline conditions. Nearly fully hydrolyzed forms result in forming PVA hydrogels with tuneable properties through crosslinking of the linear polymers which subsequently result in the polymer (gel) - fluid (sol) species. Polymer content affects the physical status of the resulting material: low polymer content results in a soft material because the fluid moves freely through the matrix while a higher polymer content results in considerable stiffening and strengthening of the material's matrix. PVA has broad applications such as in paper adhesion, packaging, medical threads, contacts, a supportive structure in 3D printing and reinforcement in structural materials, i.e., cement strengthening[30].

1.3.2 Graphene

Graphene, one of the allotropes of carbon, is a monolayer of two-dimensional honeycomb lattices of sp2 hybridized carbon atoms. It possesses very peculiar electrical properties such as anomalous quantum Hall effect and high electron mobility at room temperature.[31] In a graphene nanostructure, two carbon atoms are bonded together with a sigma (σ) chemical bond, an extremely strong bond in materials due to hybridized orbitals generated by the superposition of 2s, $2p_x$, and $2p_y$ orbitals. These planar orbitals form highly stable and localized σ bonds with the three nearest carbon atoms and mainly responsible for the presence of binding energy and the elastic properties of the graphene sheet. The $2p_z$ are the remaining "free" orbitals which are perpendicularly oriented to the molecular plane and hybridizes to form the conduction (π) and valence (π*) bands, the ones responsible for the electrical conduction of graphene. The graphene sheet is hydrophobic and forms quick agglomerates due to strong π-π interactions along the graphene surface area.[32] One possible route to harnessing these excellent properties of graphene for the application would be to incorporate graphene sheets in a composite material. The physical properties of graphene are listed in Table 4.

Table 4 Properties of graphene

Young's modulus (GPa)	400-1000	2010[33], 2014[34], 2017[35], 2018[36]
Tensile strength (GPa)	10-130	2013[37], 2014[34], 2017[35], 2018[36]
Thermal conductivity (W/m K)	5000	2018[36]
Electrical Conductivity (S/m)	100	2012[39]
Specific surface area (m^2/g)	200 - 2630	2010[34], 2013[38], 2018[36]

Graphene synthesis can be achieved via few methods, for example, mechanical cleaving or scotch tape method via exfoliation, chemical synthesis, especially the most commonly

used graphite oxidation-reduction method and chemical vapor deposition (CVD)[40] (

advantages and disadvantages are shown in Table 5). Among these methods,

simultaneous control of the average size, shape, and number of graphene layers, as well

as the scalability and mass production, are generally not satisfactory. This thesis will

concentrate on a low-cost, facile, and highly efficient exfoliation method generates one-

layer or few-layer graphene in composite fibers.

Table 5 Various techniques of graphene synthesis

Methods	Description	Advantages	Disadvantages
Liquid phase exfoliation[41,42]	use of an ultrasonic treatment for stabilizing graphite flakes in a solvent or surfactant solution.	high yield, low cost, simple scalability	structural and manufacturing defects
Mechanical peeling[43,44]	graphene is detached from a graphite crystal using adhesive tape via one-step or more often a few-step repetitive process.	simple technique, high-quality graphene.	labor intensive, low scalability, non-uniform sizes
Chemical synthesis[44,45]	oxidation-reduction of graphite or intercalated agents are penetrated between graphene layers to exfoliate graphene.	mass production	high cost, safety issues
Chemical vapor deposition[43,46]	when heated with plasma, gaseous compounds (e.g., a gas mixture of H_2, CH_4, and argon) decompose on the substrate surface (e.g., nickel, copper) to grow thin films of graphene.	well-controlled graphene sizes, shape, layers	uncertain purity, high-cost, complex transfer process

1.3.2 State-of-the-art

Several processing methods including solution mixing, simple solution casting, electrospinning, gel spinning, compression molding, and in-situ reduction have been used to fabricate PVA/graphene nanocomposite fibers by researchers as listed in table 6. Nanoparticles ranging from GNPs, FLGs, exfoliated graphene, reduced GO, BGOs, GOs, d-GO, P-GO, S-rGO, tryp-graphene, and ADS-Gs have been used. The researchers have incorporated graphene of concentrations as low as 0.1 wt% to as high as 40 wt% for mixing with PVA matrix. These different graphene types have been synthesized by various techniques that include mechanical peeling, chemical synthesis, and chemical vapor deposition. The increase in Young's modulus and tensile strength can go up to 27 GPa and 1600MPa, respectively.

Their full potential hasn't been achieved yet because of partial dispersion, incomplete alignment of graphene sheets in the polymer matrix, limited interfacial adhesion between graphene and polymer, and, the maximum graphene content the composite can accommodate to achieve the best outcome. These obstacles are associated with the inherent characteristics of graphene such as extremely low bulk density, large surface area, and high aspect ratio.[47] More research is necessary to recognize the aforementioned pitfalls, namely, the dispersion techniques to get better graphene exfoliation and reduce agglomerations, methods to increase interface strength and bring tensile and modulus values closer to theoretical values of the graphene. This research focuses on sonication methods for instant graphene dispersions, and the dry-jet wet spinning method to achieve controlled graphene morphology and dimensions, which eventually enhances the mechanical properties that include improved tensile strength and elastic modulus.

13

Table 6 PVA/ graphene-related composites

Graphene	Concentration (wt%)	Fiber fabrication method	Modulus (GPa)	Strength (GPa)	Reference
GNP	2	Solution mixing	1.5	38	2016[48]
FLG	2	Solution casting	3.83	0.09	2012[49]
Mechanically exfoliated graphene	0.3	Electrospinning	2.1		2018[50]
rGO	2	Electrospinning	0.085	0.0055	2013[51]
GO	1	Solution casting	4.5	0.1	2013[52]
BGO		Solution mixing		0.65	2014[53]
rGO	10	Solution mixing	3.25	.660	2018[36]
dGO	0.1	Gel spinning	27.2	1.58	2017[54]
rGO	0.7	Solution processing/compression molding	4.9	0.154	2014[46]
GO	0.7	Solution mixing method	3.45	0.0876	2009[55]
tryp-Graphene	0.2	Solution mixing	1.56	0.0472	2011[56]
P-rGO	0.7	Solution mixing	4.9	.154	2013[57]
S-rGO	0.5	Solution mixing	4.3	0.135	2013[57]
GO	30	Simple solution casting	13.5	0.28	2015[58]
SRGO	40	Simple solution casting	8.5	0.252	2015[58]
rGO	1.5	In-situ reduction	5.51	0.085	2014[59]
ADS-G	2.5	Simple solution casting	6.31	0.123	2014[59]

Note: GNP, graphene nano-platelets; FLG, Few layer graphene; rGO, reduced graphite oxide; GO, graphene oxide; BGO, boron cross-linked graphene oxide; dGO, poly (dopamine) coated graphene oxide; tryp-Graphene, tryptophan functionalized graphene; SRGO, sulfonated graphene oxide; P-rGO, Poly(N-vinyl-2-pyrrolidone) (PVP) stabilized rGO; ADS-G, aryl diazonium salt functionalized graphene

1.3.3   Challenges

One of the challenges in developing polymer composites for advanced technology applications is the limited ability to disperse graphene evenly in a polymer matrix, especially at high graphene concentrations. Techniques such as ultrasonicators, magnetic fields, and surfactants to enhance the dispersion of graphene have been used.[60] Several

strategies have been used to improve dispersion quality, including either chemical or physical approaches. Surface modification is often used to enhance the compatibility of the matrix and fillers for example through the grafting of organosilanes or through the use of long chains alkyl ammonium clay platelets intercalating ions. Also, in-situ polymerization may be preferred to reach a good dispersion state which is sometimes difficult to reach when processing nanocomposites in highly viscous media.[61]

The second challenge is to achieve efficient interfacial interactions due to the graphene tendency to wrap or curl surround by polymer chain. As is already known that small size of the fillers leads to a dramatic increase in interfacial area and that this area creates a significant volume fraction of interfacial polymer with properties different from the bulk polymer even at low loadings. The properties and structure of this interfacial region are not yet known quantitatively, presenting a challenge both for controlling and predicting the properties of polymer nanocomposites.[62]

The third challenge is the alignment of graphene. During dispersion and mixing with the polymer matrix, the graphene sheets fold, crumple, and bend which hampers the process of structured alignment and orientation with polymer chains.[63]

1.4   Characterization of microstructures

Some powerful techniques are available for studying the degree of exfoliation, get optimized properties/performances and microstructures, and to know their effect on the corresponding polymer nanocomposites.[64] Also they are helpful in quantifying property and structure features including mechanical, thermal, conformational, optical, and other functional behaviors.[65]

15

1.4.1 Scanning electron microscopy (SEM*)*

Electron microscopy investigates the structure, morphology and composition of polymer nanocomposites using different characterization techniques like transmission electron microscopy (TEM) and SEM.[66] In scanning electron microscopy (SEM), a beam of electrons strike the surface of the specimen and interact with the atoms of the sample, generating signals in the form of secondary electrons. Backscattered electrons and characteristic X-rays are generated which contain information about the sample's surface topography, composition and so on.[67]

1.4.2 Wide-angle x-ray diffraction (WAXD)

By this transmission experiment, the X-ray beam passes through the sample and produces a diffraction pattern which is a plot of the intensity of X-rays scattered at different angles by a sample. The X-ray detector collects the X-rays and its position is recorded as 2theta (2Ө). The crystal structure determines the position and intensity of the diffraction peaks in an X-ray scattering pattern. Each diffraction peak is attributed to the scattering from a specific set of parallel planes of atoms and Miller indices (hkl) are used to identify them. Several parameters that can be detected are listed in Table 7.

Table 7 XRD analysis important parameters

Structural features	Theory/basis	Reference
d-spacing	Bragg's law	Basics of X-ray diffraction(Speakman)[68]
Crystallinity	Ratio of diffraction (crystalline) peak area to the total of crystalline and amorphous regions	Murthy (2018)[69]
Crystal size and shape factor	Scherrer equation	Estimating crystallite size (Speakman)[70]

Note: Bragg's law, $\lambda = 2 * d_{hkl} * Sin\Theta$, where Scherrer equation, $B(2\Theta) = \frac{K * \lambda}{L * Cos(\theta)}$, where K is the dimensionless shape factor, λ is the X-ray wavelength, L is the crystallite size in Angstroms, Θ is the Bragg angle, and B is the line broadening at Full Width half Maximum (FWHM).

1.4.3 Differential Scanning Calorimetry (DSC) and Thermogravimetric Analysis (TGA)

The thermal analysis provides property information of materials as they change with temperatures. Methods including, but not limited to, differential scanning calorimetry (DSC), thermogravimetric analysis (TGA), dynamic mechanical analyzer (DMA), and thermo-mechanical analysis (TMA) are used. Based on the parameters measured, DSC monitors the heat difference, TGA examines the mass upon heating, DMA examines the mechanical stiffness and damping with thermal scanning, and TMA probes the dimensional changes during shrinking/expansion. For polymer-based materials, DSC, TGA, and DMA provide crystallization, environmental resistant behaviors such as glass transition and degradation temperatures, and content regarding alternative phases present in composites.

1.4.4 Static mechanical tests

Static mechanical test includes methods such as stretching, compressing, bending, and indenting samples without any coupled exterior field. The tested parameters include modulus, strength, yield, fracture strain etc.

CHAPTER 2 MATERIALS AND EXPERIMENTAL METHODS

2.1. Materials

2.1.1 Nanoparticles

Graphene nanoplatelets grade C-750 is purchased from Sigma Aldrich with bulk density 0.2-0.4 g/cm^{-3}, relative gravity 2–2.25 g/cm^{-3} average in-plane dimensions ⩽ 2 um and surface area = 750 m^2/g. The microstructure of GNPs look like as shown in figure 4.
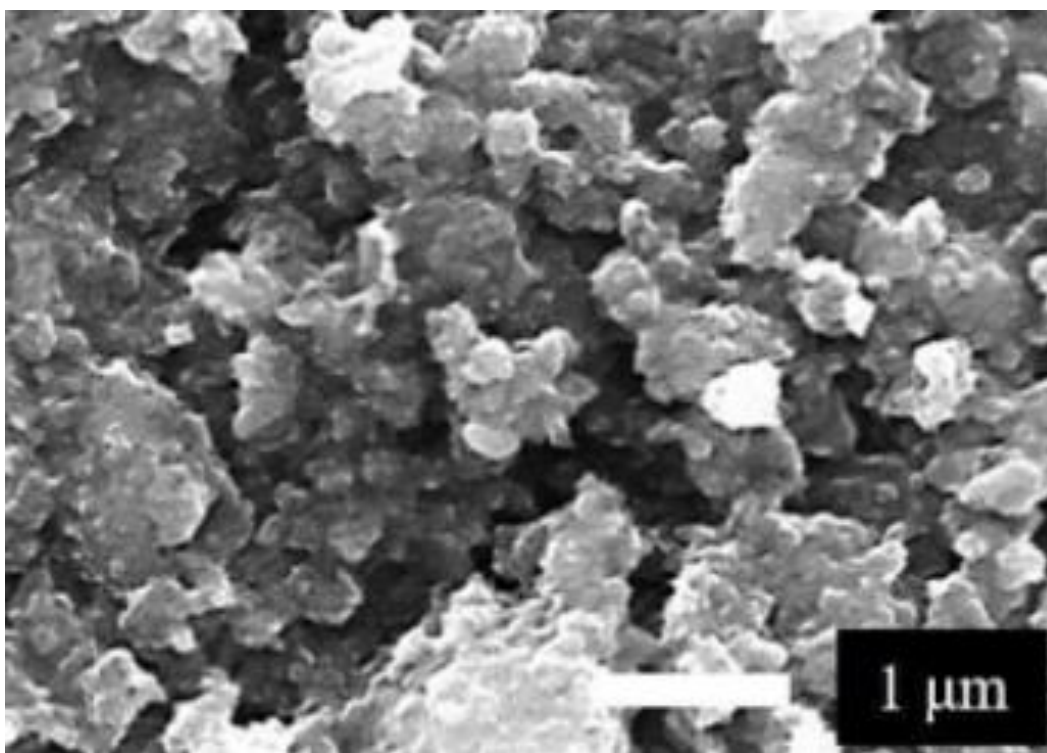
Figure 4 SEM showing microstructure of GNP particles

2.1.2 Polymers

PVA Kuraray 28–98 (M$_w$ ~ 145,000 g/mol and degree of hydrolysis 98-99%) was purchased from Kuraray. 20 gram of PVA granules were dispersed in 100 ml dimethyl sulphoxide (DMSO) and stirred using a mechanical stir for 2 hours at room 150˚C.

2.1.3 Dispersion of nanoparticles

8 gram of graphene nanoplatelets (GNP) powder was dispersed in 40 ml dimethyl sulphoxide (DMSO) and stirred using a magnetic stir for 20 minutes at room temperature. The dispersion was then sonicated for 15 minutes using a tip sonicator (brand) with 40% amplitude. Room temperature was maintained by resting for 5 seconds after every 5 seconds of sonication. The obtained dispersed GNPs looked like as shown in figure 5.
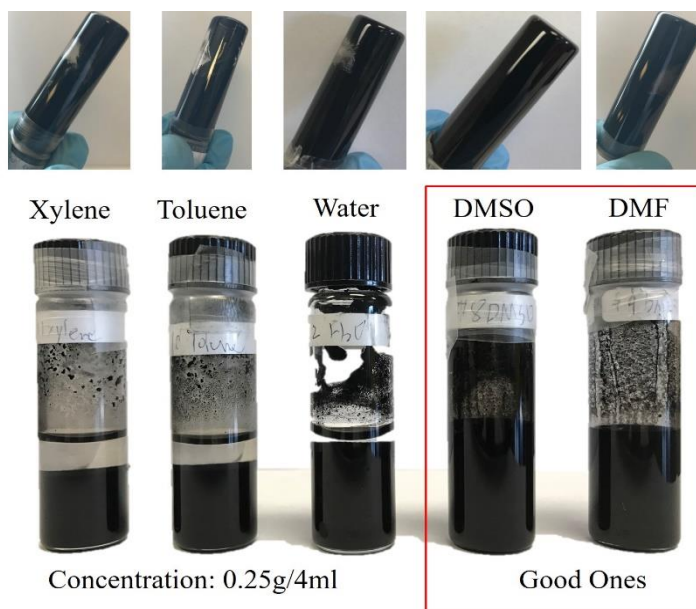
Figure 5 Dispersion of graphite nanoplatelets (GNP) in different solvents of xylene, toluene, water, dimethyl sulfoxide (DMSO), and dimethylformamide (DMF)

Several solvents have been identified for dispersing graphene, in particular NMP, DMSO, and DMF. For solvent interactions with graphene, the following results were obtained through the recent molecular dynamics simulation[71]:

$$NMP{\sim}DMSO{>}DMF{>}Xylene{>}Toluene{>}Water$$
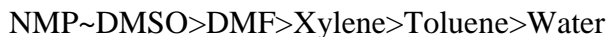
NMP and DMSO exhibit similar traits from a good solvent perspective.[71] As prepared GNP dispersions in four organic solvents (DMSO, ethylene glycol, DMF, NMP, and THF) exhibit long-term stability comparable to that observed for the dispersion of the

same material in water.[72] The Gibbs energy of mixing a species and solvent per unit volume (ΔGmix) is given by

$$\Delta G_{mix} = \Delta H_{mix} - T\Delta S_{mix} \text{--------------------------------(1)}$$

where T is temperature; ΔH_{mix} and ΔS_{mix} are the enthalpy and entropy, respectively, of mixing per unit volume. ΔS_{mix} will be positive, although small, for a rigid structure like graphene.[73] DMSO and DMF, being good solvents minimize the enthalpic cost of mixing, from equation (1), and in turn the thermodynamic instability of these dispersions, by having similar surface energy to graphene nanoplatelets. The surface energy of graphene is estimated to be ca. 68 m J m^{-2}, which is very close to DMSO.[73] PVA is also readily soluble in polar solvents like DMSO, which is reported to be a better solvent for PVA than water. The intrinsic viscosity of PVA in DMSO is observed to be higher (3.25 dL/g) than in water (0.93 dL/g). The high molecular weight of DMSO and high degree of its interaction with PVA causes PVA chains to remain in extended conformation compared to that in water.[74]

2.1.4   Preparation of PVA-GNP suspensions

Fiber spinning was done using a syringe pump and syringe needle. PVA-DMSO dope and dispersed homogeneous graphene solution were added to different syringe needles (diameter 1 mm) and controlled by different syringe pumps. Syringe operation was controlled for 1-phase, 2-phase, and 3-phase at different rates as shown in Table 8. The as-spun dispersion formed a gel in the methanol bath. Gel fiber was continuously collected on a fiber take-up unit. The gel fiber was kept immersed in a methanol bath for more than 6 hours before drawing on a hot plate at 100°C, 150°C, and 200 °C.

Table 8 Spinning parameters input data

Fiber Type	Syringe piston diameter	Syringe volume	Injection rate
1-phase	PVA-DMSO (19mm)	30 ml	3 ml/min
2-phase	PVA-DMSO (28mm)	100 ml	3 ml/min
	GNP-DMSO (19 mm)	30 ml	1ml/min
3-phase	PVA-DMSO (28mm) (Two needles)	100 ml	3ml/min
	GNP-DMSO (19 mm)	30 ml	0.5 ml/min

2.2 Structural formation in fibers

Fiber spinning is the process of converting the polymers in the form of melts or solutions into the fibers. The fiber forming material could be in a liquid/semi-liquid/concentrated state, which is then extruded through the spinneret, and then returned to the solid state by solidification into fiber form. This thesis involves the dry-jet wet spinning/gel-spinning process. The gel-spinning involves spinning dopes in the form of gels, which keeps the polymer chain bounds together and produces high-strength polymer fibers. These polymers include polyacrylonitrile (PAN) and ultra-high molecular weight polyethylene (UHMWPE) as well as polyvinyl alcohol (PVA) that is going to be studied in this study. The polymer solution or gel is extruded from the spinnerets in fiber forms, cooled in a nonsolvent or water, and stretched into gel fiber by ultra-high extension. During the process of cooling, the polymer solution will gradually lose the solution mobility, which is known as the gelation of the polymers. This allows the individual molecular chains in solution to connect optimally with each other, and on coagulation, form a network structure. As the new forming fiber contains a large amount of solvent and is in the gel state, it requires ultra-drawing to produce the ultra-high strength and high modulus fiber.[75]

The general gel spinning process can be subdivided into the following four steps:

2.2.1 Dissolution

First, the polymer is dissolved in the solvent to prepare a homogeneous dope. The molecular chains of the solid polymers may be entangled and the entanglements will affect the molecular chain stretching. In the dilute solution, the entanglement density is very low, the stresses applied during spinning and drawing do not completely transfer from one chain to another chain because of poor connectivity, and the molecular chains remain in coiled or folded configuration. This results in poor spinnability. This means that for making fibers with enhanced properties from flexible polymers, the spinning process should be modified in such a manner that it allows the formation of fully extended and oriented polymer chains. In semi-dilute and concentrated solution within an appropriate solvent, the polymer molecular chains are forced into extended chain structure using physical interactions in the gel state. Also, in this state just sufficient entanglements exist between polymer chains, thus the spinning stresses are able to transfer to all the chains without any hindrance. Such an optimum level of entanglement density facilitates high drawability of the polymer network. Figure 7(a) exhibits the dissolution process wherein the PVA and DMSO are being mechanically stirred.

2.2.2 Spinneret injection

The PVA solution has unique non-Newtonian behavior. At lower spinning speed, the extruded solution exhibits quite a large die swell, which is related to PVA solution's high elastic property. With increasing spinning speed, the size of die swell become smaller due to the stretching under the spinneret, and at much higher spinning speed, a phenomenon known as "pull-out" is observed up to filament breakage. This typical behavior is due to the combination of higher elongation strength of the solution and its high elastic property.

23

When the solution is pressed through the spinneret and the strain is applied, the molecules are forced into a highly elongated form. This forms the first step in the orientation process (Figure 6).
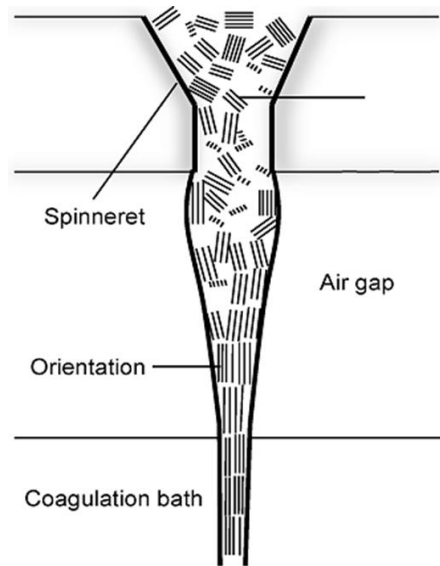
Figure 6 The morphology of fibers during spinning

Fibers are extruded from the spinneret through a gear pump and cooled rapidly by air or water. The rapid cooling process can lead to the formation of the crystals and the crystallization begins. During the crystallization process, some of the entanglements are lost because the chain will be disentangled before crystallization. Therefore, all entanglements can't be incorporated in the crystal and this is another reason for the success of gel spinning even at high concentration. The retention of the disentangled state of polymers aids in the formation of high strength and high elastic modulus fibers. Through the crystallization process, the solution is solidified into a more rigid gel-like structure having dispersed crystallites connected by a small number of entanglements remaining as pseudo crosslinking points. Such a structure is ideal for the drawing. The

injection process is exhibited by figure 7 (b) wherein three syringes are shown, two for PVA and one for GNPs.

2.2.3   Coagulation

During the dry-jet wet spinning process, the solution of fiber-forming material is extruded into the air before entering coagulating bath that causes the jets to harden as a result of the chemical or physical change. A coagulant is used in the coagulation bath to remove the solvent from the spun fibers. To achieve this, the natural drying method and the use of extractant are the most common methods. The extractant is primarily used to remove the solvent residuals from the gel fiber. In gel-spinning, the selection of solvent and extractant directly affect the stretching ability and is key to the gel spinning process. After removal of the solvent, the fiber consists of microcrystalline crystals embedded in the non-crystalline material. Figure 7c gives a glimpse on the coagulation apparatus an process for the dry jet wet spinning. The effect of coagulation can be seen in figure 8, where the microcrystalline sructures are embedded polymer chains. In the subsequent drawing stage, the apparently random crystals and most of the non-crystalline material is transformed into a highly crystalline, highly oriented fiber.[76]

2.2.4   Stretching and drawing

The final properties of the fiber in the gel spinning process are achieved in the drawing stage. The strength and modulus are directly related to the draw ratio. The maximum attainable draw ratio is related to the molecular weight and the concentration. The attainable draw ratio increases with decreasing concentration, however for each molecular weight there is a minimum concentration below which drawing isn't possible

due to insufficient molecular overlap. The drawing behavior is related to the number of chain-chain entanglements. The drawing involves the high magnification stretching of the gel fiber. It can change the folded polymer molecular chains to straight chains and improve polymer crystallinity and orientation. It's a unique feature of gel spinning and the key to enhancing gel fiber performance.[75] Figure 7(d) shows the lab apparatus for drawing fibers through hot plate. The morphology of a drawn fiber with aligned fillers is as shown in figure 6.
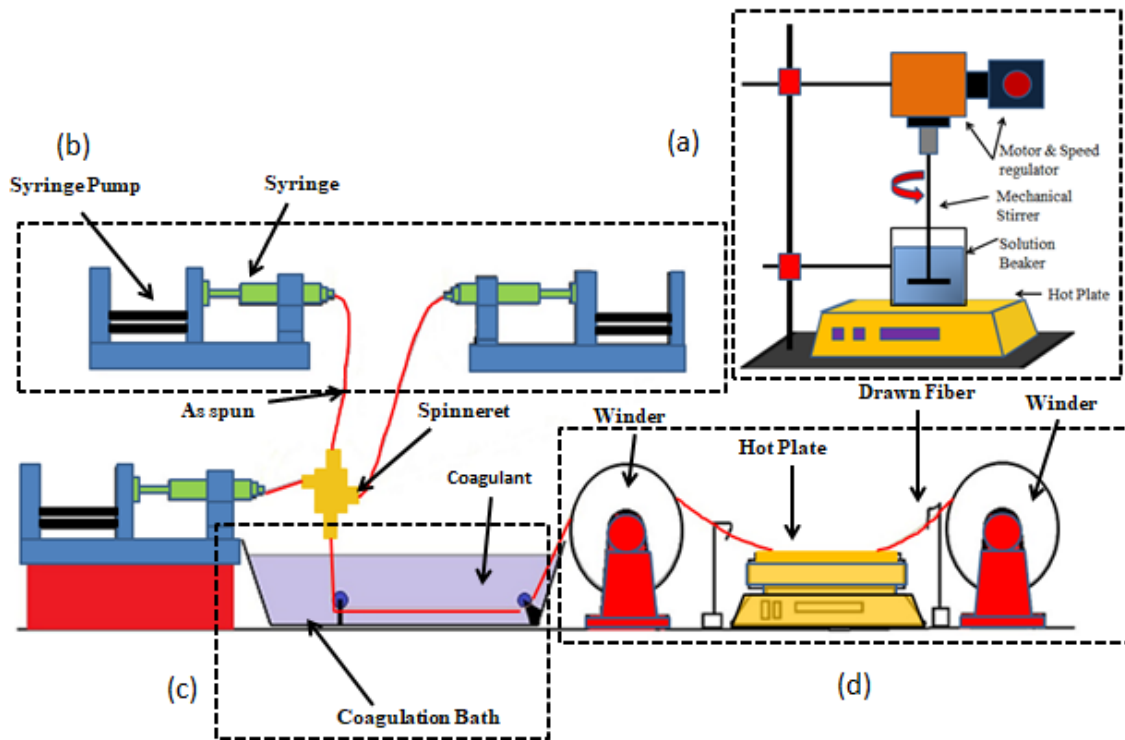
Figure 7 Apparatus setting for the spinning and drawing process (a) solution preparation (b) injection (c) coagulation (d) drawing

2.3 Spinneret engineering

The spinning of the polymer into filaments involves two types of fluid flow:

1) shear flow before the extrusion i.e., flow through a spinneret,

2) elongational flow (extensional flow).

These flows have to be in a stable region in order for the spinning to occur without defects or breaks in the spun filament. In most polymer production operations, the production rate is often limited by the onset of flow instabilities. Therefore, understanding the causes of fluid instabilities is important for the successful polymer fluid spinning.

semi dilute
solution

gel
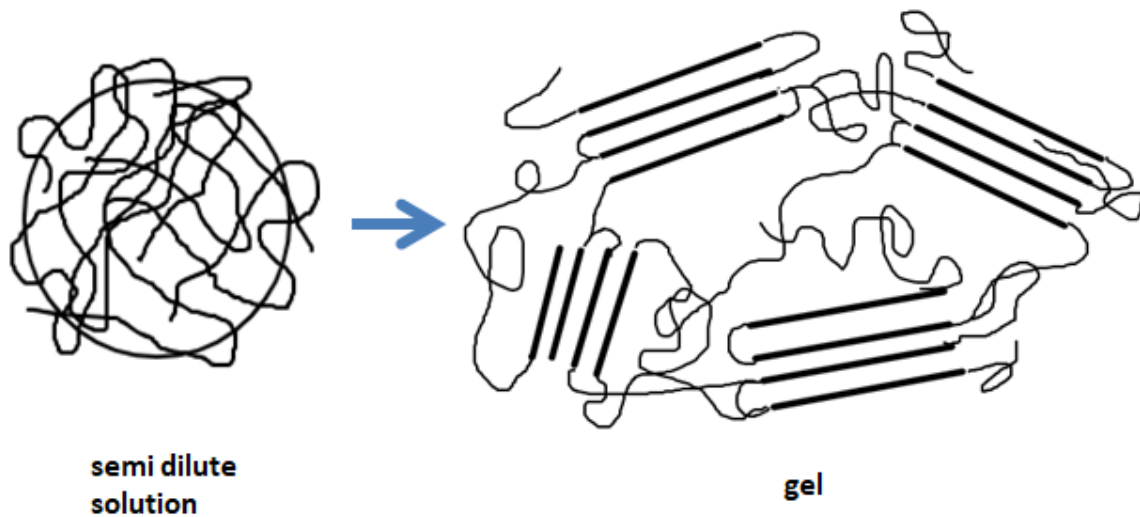
Figure 8 Internal morphology of solutions

The spinnerets used in the production of most manufactured fibers are similar to a shower head and they may have one to several hundred holes. As the filaments emerge from the holes in the spinneret, the liquid polymer is converted first to a rubbery state and then solidified. This process of extrusion and solidification of endless filaments is called spinning. Spinneret is the starting position where the spinning dope begins to form tow,

27

which is the key part for forming tow, and the initial spinning conditions will greatly affect the fiber geometrically and mechanically.[76]

For research purpose, the spinneret is designed on Creo Direct Express 6.0. Three different models are created to accommodate the needs of spinning PVA, core-shell 2-Phase and 3-phase fibers. For PVA fibers, only one input and output is necessary as shown in figure 9(a). For 2-phase, two inputs, one for PVA solution and the other for GNP solution is provided (as shown in figure 9(b) and for 3-phase, three inputs have been provided, one for GNPs and two for PVA solution (as shown in figure 9(c)).
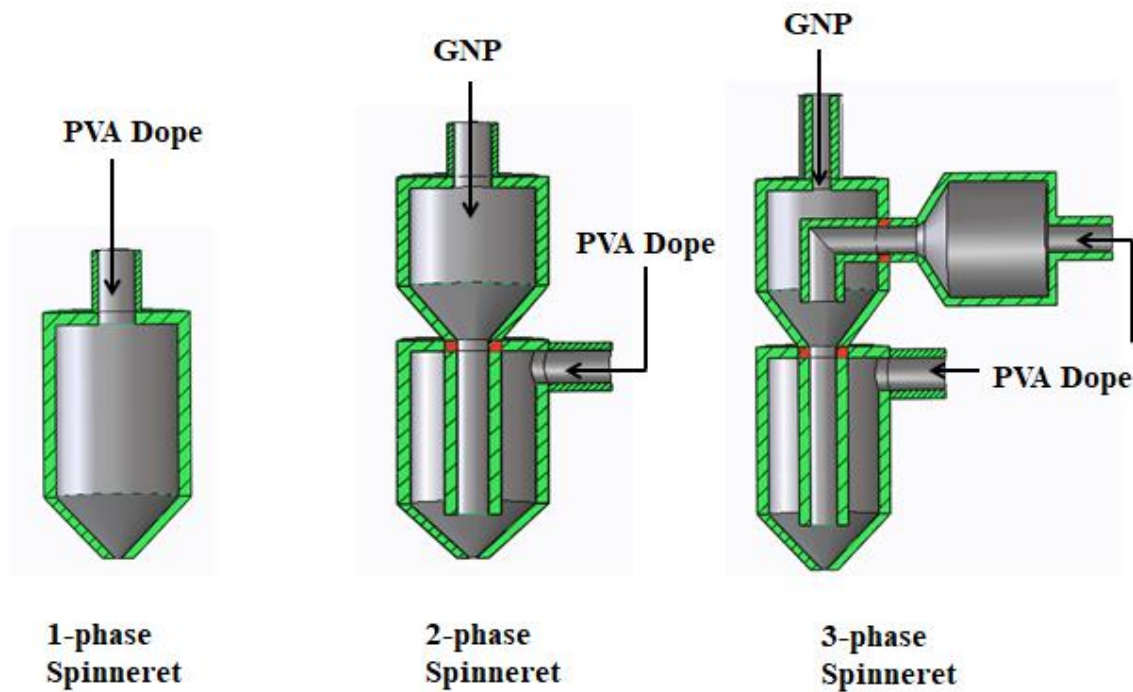
Figure 9 (a) 1-phase spinneret (b) 2-phase spinneret (c) 3-phase spinneret

The spinneret hole was supposed to achieve a fiber diameter on a length scale of micrometers, but due to the limitations of 3D printing technology, the least diameter

achievable and feasible to fabricate co-axial fibers was 1mm. This design allows the multi-material inclusion i.e., the core-shell or laminate structures.

CHAPTER 3 RESULTS AND DISCUSSION

The microstructures and properties of the obtained polymer and composite fibers have been characterized using TGA, DSC, WAXD, and tensile testers.

3.1   Thermal gravimetric analysis and Diffraction scanning calorimetry

TGA/DSC (LABSYS EVO) was used to for all fiber analysis. The samples were placed in an alumina crucible along with an alumina sample as reference. The chamber was purged with helium gas at 0.5 °C/min for 30 mins and was heated under a rate of 10 °C/min up to 600 °C. As shown in Figures 10 and 11, the graphene concentrations in 2-phase fiber and 3-phases fibers are around 4 wt% and 20 wt%.
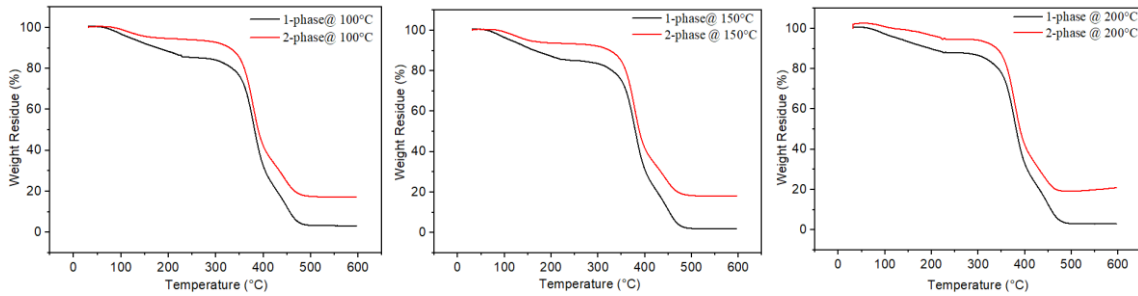
Figure 10 TGA result comparing 1-phase with 2-phase at 100˚C, 150˚C, 200˚C
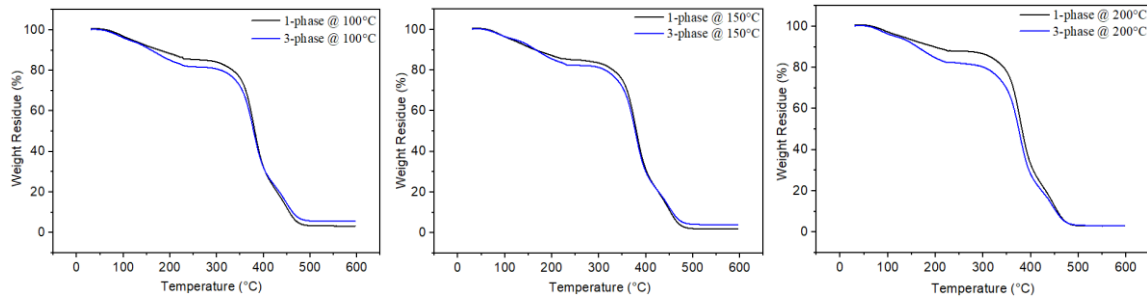
Figure 11 TGA result comparing 1-phase with 3-phase at 100˚C, 150˚C, 200˚C

3.2 Wide angle x-ray diffraction (WAXD)

X-ray diffraction patterns of samples were obtained by a wide angle X-ray diffractometer (XRD, Kristallo-Flex 710D X-ray generator, Bruker D5000, Siemens) with Cu Kα radiation (40 kV, 40 mA). The scanning range of the Bragg 2θ angle ranged from 5° to 70° under a scanning rate of 2° min^{-1}. 1-phase, 2-phase, and 3-phase fibers were analysed and Intensity vs 2theta plots were generated as shown in Figure 12, 13, and 14. The crystallinity degree of polymer and composite fibers are summarized in Table 9, suggesting the higher crystallinity of 3-phase fibers than the 2-phase and PVA fibers.
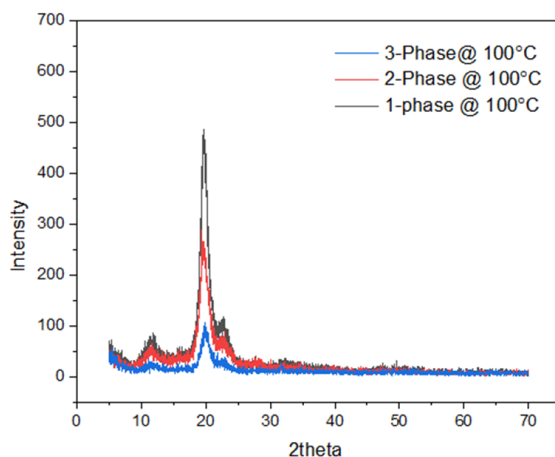
Figure 12 WXRD plots of 1-phase, 2-phase, and 3-phase fibers at 100˚C
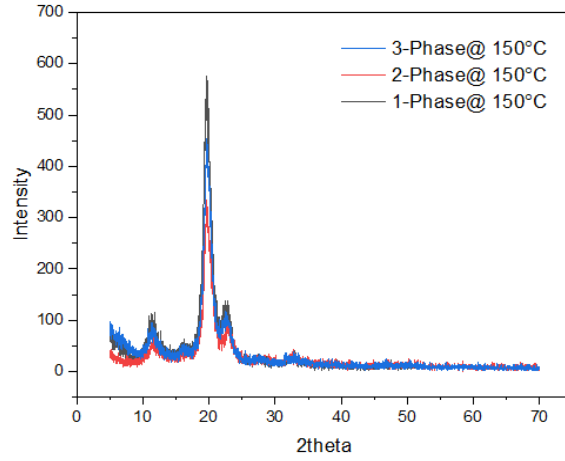
Figure 13 WXRD plots of 1-phase, 2-phase, and 3-phase fibers at 150˚C
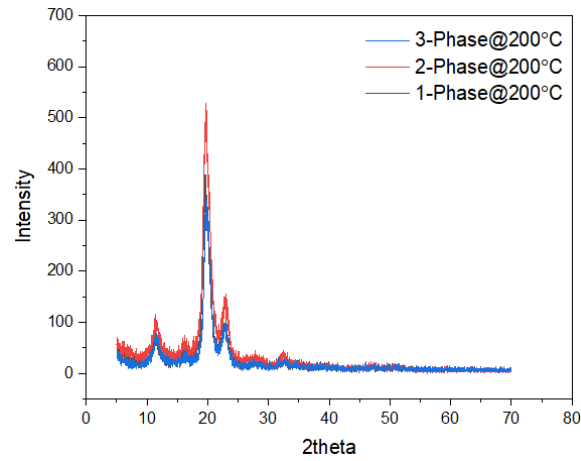
Figure 14 WXRD plots of 1-phase, 2-phase, and 3-phase fibers at 200˚C

Table 9 Crystallinity in 1-phase, 2-phase, and 3-phase fibers

	100	150	200
1-phase	67.64	83.95	66.81
2-phase	52.3	76.54	81.42
3-phase	48.7	80.68	86.02

3.3   Mechanical Test

The tensile test was performed using Instron® 3300 series electromechanical universal testing machine (Norwood, MA, United States) with the cross head speed of 15 mm/min. The initial length was 5 mm. The number of the test specimens was at least 10 for each sample. Tensile modulus, tensile strength, tensile strain were directly measured. 1-phase, 2-phase, and 3-phase fibers were stretched until they broke and tensile stress vs tensile strain plots were generated (Tables 10, 11 and 12, and Figures 15, 16 and 17). The data in Tables 10 to 12 clearly showed that the introduction of nanoparticles could improve the mechanical parameters of elastic modulus and tensile strength although the tensile strains in the composites are smaller than that in the pure polymer fibers. Moreover, the 3-phase fibers showed better mechanical properties than the 2-phase fibers although the graphitic fillers are higher in former, namely, 20 wt% in 2-phase fibers and 4 wt% in 3-phase fibers. The obtained mechanical data is compared with data from other literature studies as shown in figure 18.

Table 10 Tensile test results at 100˚C

Temperature	Modulus (GPa)	Tensile Strength (MPa)	Tensile Strain (mm/mm)%
1-phase	0.22±0.03	53.77±5.75	160±0.1
2-phase	1.04±0.11	286.88±29.44	42±0.07
3-phase	4.04±0.3	365.13±21.77	61±0.04

Table 11 Tensile test results at 150˚C

Temperature	Modulus (GPa)	Tensile Strength(MPa)	Tensile Strain (mm/mm) %
1-phase	0.38±0.05	120.39±10.32	46±0.08
2-phase	2.53±0.16	326.59±15.93	21±0.02
3-phase	9.95±0.28	422.76±22.92	23±0.07

Table 12 Tensile test results at 200˚C

Temperature	Modulus (GPa)	Tensile Strength (MPa)	Tensile Strain (mm/mm) %
1-phase	4.04±1.519	145.52±2.91	10±0.01
2-phase	2.8±0.08	358.23±30.88	16±0.00
3-phase	15.64±1.33	427.00±52.34	16±0.02

A simple analysis based on mechanics models such as the Rule-of-the-mixture or Halpin-Tsai generated the modulus prediction of graphene, i.e., 530.3 GPa assuming graphene alignment and 1400.0 GPa for randomly distributed fillers. Known from the theoretical values that the graphene displays an intrinsic modulus up to 1000 GPa, the graphene in this study cannot be randomly aligned. Table 13 exhibits the composite mechanics analysis performed for the 3-phase 200˚C fibers.
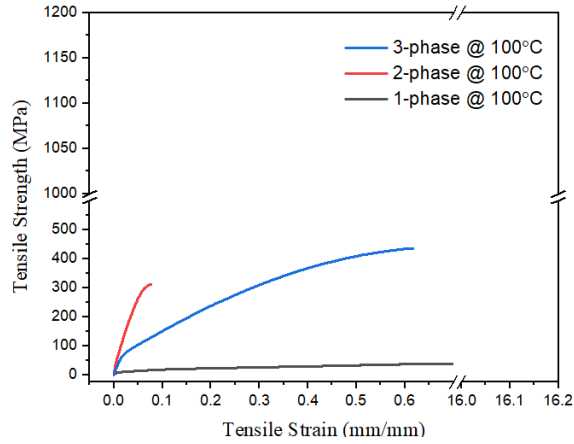
Figure 15 Tensile stress vs. strain plots 1-phase, 2-phase, and 3-phase fibers at 100˚C
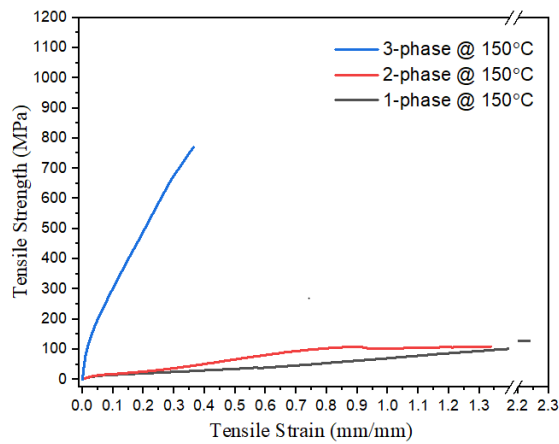
Figure 16 Tensile stress vs. strain plots 1-phase, 2-phase, and 3-phase fibers at 150˚C
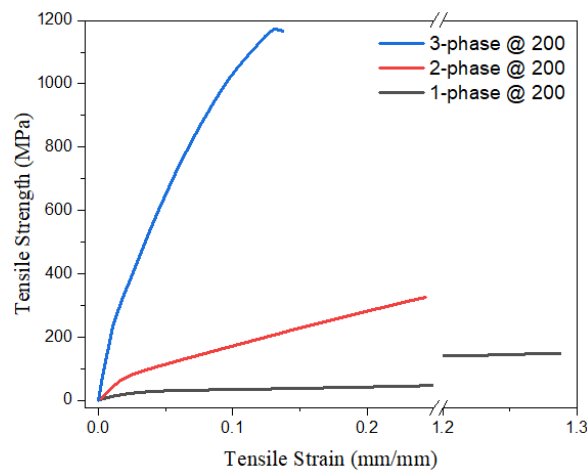
Figure 17 Tensile stress vs. strain plots 1-phase, 2-phase, and 3-phase fibers at 200˚C

Table 13 Composite mechanics analysis for 3-phase 200˚C drawn fibers

Theories	Formulas	Predicted graphene filler modulus (GPa)	Samples
Rule-of-mixture	$E_c = E_m V_m + E_f V_f$	530.3	3-phase
Halpin-Tsai model in calculating lower bound modulus for randomly aligned particle reinforcement	$E_c = E_m [\frac{3}{8}(\frac{1 + \frac{\frac{E_f}{E_m} - 1}{\frac{E_f}{E_m} + e} e V_f}{1 - \frac{\frac{E_f}{E_m} - 1}{\frac{E_f}{E_m} + e} V_f}) + \frac{5}{8}(\frac{1 + 2\frac{\frac{E_f}{E_m} - 1}{\frac{E_f}{E_m} + 2} V_f}{1 - \frac{\frac{E_f}{E_m} - 1}{\frac{E_f}{E_m} + 2} V_f})]$	1400.0	

Note: PVA modulus is 4.04 GPa, 3-phase graphene concentration is 5 wt% (2.02 vol%); where E and V stand for the modulus and volume fraction for composites (i.e., E_c and V_c) and fibers (i.e., E_f and V_f). ε stands for the aspect ratio of incorporated nanotubes.
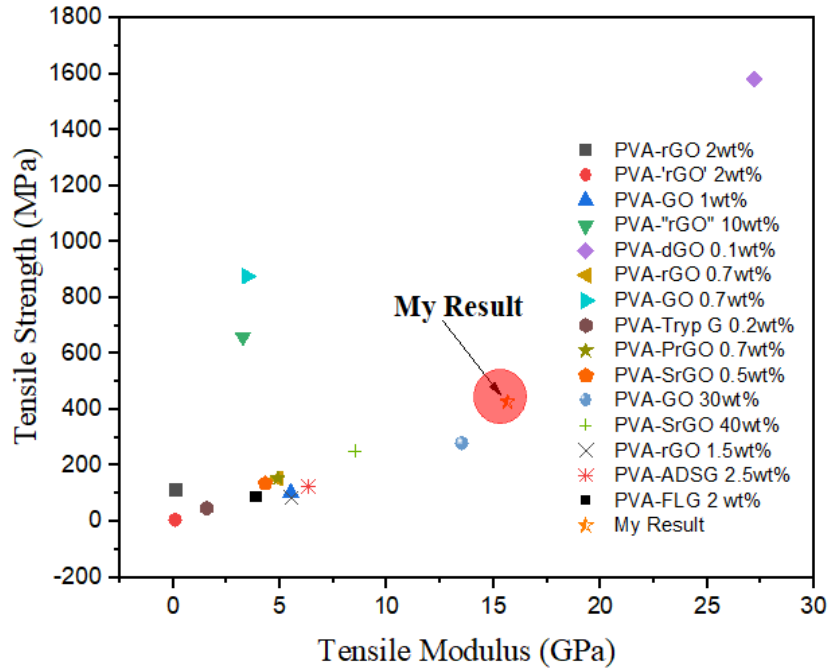
Figure 18 Summary of Young's modulus and tensile strength properties for various PVA/graphene composites produced at the research scale (Note: References available in Table 6)

3.4   Scanning electron microscopy (SEM)

SEM (XL30 ESEM-FEG) was used to obtain visual conformation on the coaxial and tri-axial fiber structures. All fibers were cooled with liquid nitrogen for 5 minutes prior to cutting into 2 cm long fibers, and were mounted on 45º mount pins for cross-sectional examination. A 15 nm gold layer was deposited on the surface to improve the conductivity. Energy of 10 KV was used for all fibers.

Figure 19 shows all fiber cross-sections, suggesting the successful fabrication of 1-phase, 2-phase core-shelled structure and 3-phase co-axial laminations. The pores/voids noticeable in 2-phase fibers could have been manifested due to multiple hypothetical reasons. During coagulation, DMSO might have exchanged with methanol and later heating-drawn stages may have evaporated the methanol leaving voids in the graphitic regions. In comparion, the 3-phase fibers showed a denser graphtic content, mainly due to the constraining of polymers in the interior and exterior regions of graphite. The existence of polymers on both sides of graphene materials can potentially facilicate the alignment of 2D graphene sheets and improve the mechanical stiffness and strength. Figure 20 showed the images of cross-section areas after tensile tests, confirming the brittle fracture in 2-phase fibers and loose state of graphite. Fractured cross-section of 3-phase fibers showed finer fibril structure and distinct graphite regions that can reinforce the polymers in sandwiched layers.
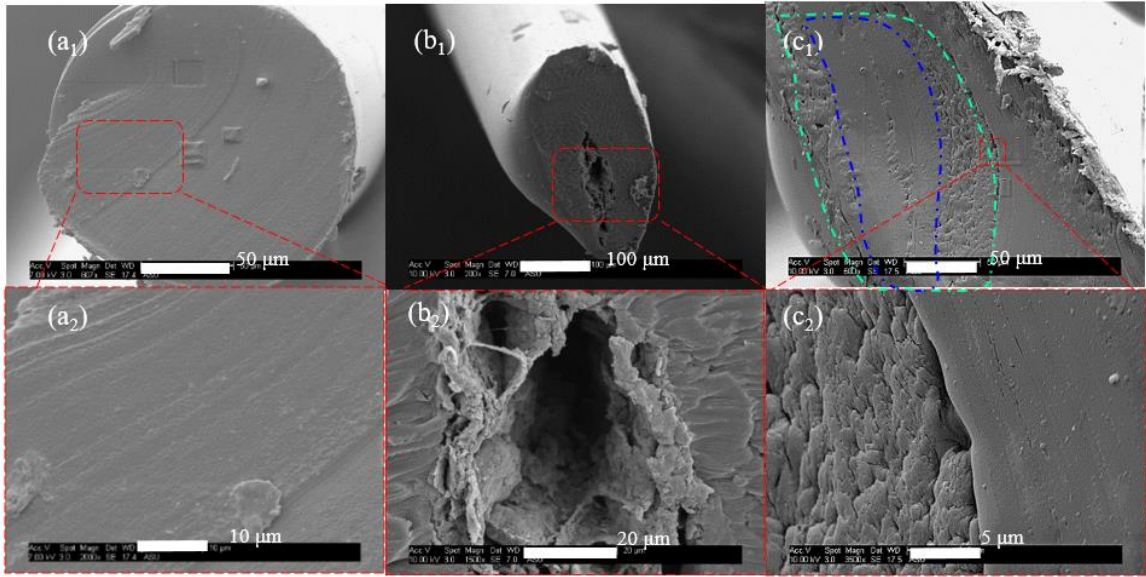
Figure 19 SEM results for the fractured surface showing differnet phases in (a) PVA and (b-c) composite fibers .
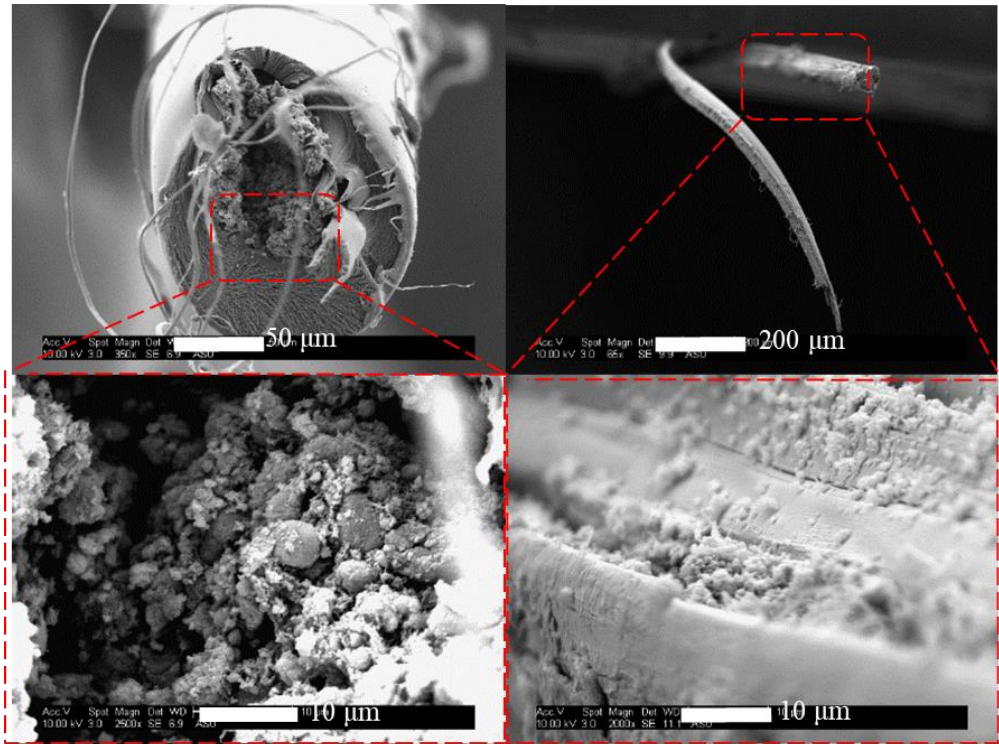
Figure 20 SEM cross section for the fracture surfaces in 2-phase and 3-phase fibers

CHAPTER 4 CONCLUSION

The primary conclusion of this study of PVA/graphene nanocomposites is that the engineered spinnerets are effective in spinning 1-phase, 2-phase, and 3-phase fibers. The composite fibers showed improved mechanical properties and modified microstructures. The 3-phase fibers have achieved enhanced mechanical properties i.e., ~15.64 GPa of tensile modulus and ~427.00 MPa of tensile strength, and in comparison to neat 1-phase PVA fibers, 3-phase fibers have an increase of 4 times in modulus. This high increase may be due to the crystallinity change in polymers and graphitic layer alignment, as shown from mechanics analyses. The 3-phase fibers showed less defective microstructures from SEM, suggesting the facilitation of graphite constraining during fiber fabrications. The future research will provide quantitative evidence for graphitic layer exfoliations and orientations.

REFERENCES

(1) Bhattacharya, Sati N. Kamal, Musa R. Gupta, R. K. *2.3 Polymer Matrices: Thermoplastics, Thermosets, Elastomers, Natural, and Biodegradable Polymers - Knovel*; Hanser Publishers, 2008, 29-30.

(2) Xu, D.; Di. The Role of Nanofillers in Polymer Nanocomposites. *ProQuest Diss. Theses; Thesis (Ph.D.)--State Univ. New York Stony Brook, 2016.; Publ. Number AAT 10193042; ISBN 9781369504156; Source Diss. Abstr. Int. Vol. 78-08(E), Sect. B.; 93 p.* 2016.

(3) Wu, S.; Peng, S.; Wang, C.; Wu, S.; Peng, S.; Wang, C. H. Multifunctional Polymer Nanocomposites Reinforced by Aligned Carbon Nanomaterials. *Polymers (Basel).* 2018, *10* (5), 542.

(4) Morimune, S.; Kotera, M.; Nishino, T.; Goto, T. Uniaxial Drawing of Poly(Vinyl Alcohol)/Graphene Oxide Nanocomposites. 2014, 38-45.

(5) Jan, R.; Habib, A.; Akram, M. A.; Zia, T.-H.; Khan, A. N. Uniaxial Drawing of Graphene-PVA Nanocomposites: Improvement in Mechanical Characteristics via Strain-Induced Exfoliation of Graphene. *Nanoscale Res. Lett.* 2016, *11* (1), 377.

(6) P. Miaudet, †; S. Badaire, †; M. Maugey, †; A. Derré, †; V. Pichot, ‡; P. Launois, ‡; P. Poulin, *,† and; C. Zakri*, †. Hot-Drawing of Single and Multiwall Carbon Nanotube Fibers for High Toughness and Alignment. 2005, 5(11):2212-5.

(7) Wu, S.; Ladani, R. B.; Zhang, J.; Bafekrpour, E.; Ghorbani, K.; Mouritz, A. P.; Kinloch, A. J.; Wang, C. H. Aligning Multilayer Graphene Flakes with an External Electric Field to Improve Multifunctional Properties of Epoxy Nanocomposites. *Carbon N. Y.* 2015, *94*, 607–618.

(8) Wang, Z. Alignment of Graphene Nanoribbons by an Electric Field. *Carbon N. Y.* 2009, *47* (13), 3050–3053.

(9) Lin, X.; Shen, X.; Zheng, Q.; Yousefi, N.; Ye, L.; Mai, Y.-W.; Kim, J.-K. Fabrication of Highly-Aligned, Conductive, and Strong Graphene Papers Using Ultralarge Graphene Oxide Sheets. *ACS Nano* 2012, *6* (12), 10708–10719.

(10) Lin, F.; Yang, G.; Niu, C.; Wang, Y.; Zhu, Z.; Luo, H.; Dai, C.; Mayerich, D.; Hu, Y.; Hu, J.; et al. Planar Alignment of Graphene Sheets by a Rotating Magnetic Field for Full Exploitation of Graphene as a 2D Material. *Adv. Funct. Mater.* 2018, *28* (46), 1805255.

(11) Ma, W.-T.; Kumar, S. R.; Hsu, C.-T.; Shih, C.-M.; Tsai, S.-W.; Yang, C.-C.; Liu, Y.-L.; Lue, S. J. Magnetic Field-Assisted Alignment of Graphene Oxide Nanosheets in a Polymer Matrix to Enhance Ionic Conduction. *J. Memb. Sci.* 2018, *563*, 259–269.

(12) Krisztián Kordás, *, †; Tero Mustonen, †; Géza Tóth, †; Jouko Vähäkangas, †; Antti Uusimäki, †; Heli Jantunen, †; Amita Gupta, ‡; K. V. Rao, ‡; Róbert Vajtai, § and; Ajayan⊥, P. M. Magnetic-Field Induced Efficient Alignment of Carbon Nanotubes in Aqueous Solutions. 200**7**, *19* (4), 787–791.

(13) Gupta, V. B. Melt-Spinning Processes. In *Manufactured Fibre Technology*; Springer Netherlands: Dordrecht, 1997; pp 67–97.

(14) Edie, D. D.; Dunham, M. G. Melt Spinning Pitch-Based Carbon Fibers. *Carbon N. Y.* 1989, *27* (5), 647–655.

(15) Weise, B.; Völkel, L.; Köppe, G.; Schriever, S.; Mroszczok, J.; Köhler, J.; Scheffler, P.; Wegener, M.; Seide, G. Melt- and Wet-Spinning of Graphene-Polymer Nano-Composite Fibres for Multifunctional Textile Applications. *Mater. Today Proc.* 2017, *4*, S135–S145.

(16) Imura, Y.; Hogan, R. M. C.; Jaffe, M. Dry Spinning of Synthetic Polymer Fibers. *Adv. Filam. Yarn Spinn. Text. Polym.* 2014, 187–202.

(17) Tian, Q.; Xu, Z.; Liu, Y.; Fang, B.; Peng, L.; Xi, J.; Li, Z.; Gao, C. Dry Spinning Approach to Continuous Graphene Fibers with High Toughness. *Nanoscale* 2017, *9* (34), 12335–12342.

(18) Clarkson, C. M.; Youngblood, J. P. Dry-Spinning of Cellulose Nanocrystal/Polylactic Acid Composite Fibers. *Green Mater.* 2018, *6* (1), 6–14.

(19) Ozipek, B.; Karakas, H. Wet Spinning of Synthetic Polymer Fibers. *Adv. Filam.*

Yarn Spinn. Text. Polym. 2014, 174–186.

(20) Puppi, D.; Chiellini, F. Wet-Spinning of Biomedical Polymers: From Single-Fibre Production to Additive Manufacturing of Three-Dimensional Scaffolds. *Polym. Int.* 2017, *66* (12), 1690–1696.

(21) Park, S. K.; Farris, R. J. Dry-Jet Wet Spinning of Aromatic Polyamic Acid Fiber Using Chemical Imidization. *Polymer (Guildf).* 2001, *42* (26), 10087–10093.

(22) Hauru, L. K. J.; Hummel, M.; Michud, A.; Sixta, H. Dry Jet-Wet Spinning of Strong Cellulose Filaments from Ionic Liquid Solution. *Cellulose* 2014, *21* (6), 4471–4481.

(23) Kim, J. W.; Lee, J. S. Effect of Heat Drawing Process on Mechanical Properties of Dry-Jet Wet Spun Fiber of Linear Low Density Polyethylene/Carbon Nanotube Composites. *Int. J. Polym. Sci.* 2017, *2017*, 1–9.

(24) Robb, B.; Lennox, B. The Electrospinning Process, Conditions and Control. *Electrospinning Tissue Regen.* 2011, 51–66.

(25) Ramakrishna, S.; Fujihara, K.; Teo, W.-E.; Yong, T.; Ma, Z.; Ramaseshan, R. Electrospun Nanofibers: Solving Global Issues. *Mater. Today* 2006, *9* (3), 40–50.

(26) Bhardwaj, N.; Kundu, S. C. Electrospinning: A Fascinating Fiber Fabrication Technique. *Biotechnol. Adv.* 2010, *28* (3), 325–347.

(27) Daristotle, J. L.; Behrens, A. M.; Sandler, A. D.; Kofinas, P. A Review of the Fundamental Principles and Applications of Solution Blow Spinning. 2016, *8* (51), 34951–34963.

(28) Medeiros, E. S.; Glenn, G. M.; Klamczynski, A. P.; Orts, W. J.; Mattoso, L. H. C. Solution Blow Spinning : A New Method to Produce Micro-and Nanofibers from Polymer Solutions. 2009, pp 2322–2330.

(29) Hofmann, E.; Krüger, K.; Haynl, C.; Scheibel, T.; Trebbin, M.; Förster, S. Microfluidic Nozzle Device for Ultrafine Fiber Solution Blow Spinning with Precise Diameter Control. *Lab Chip* 2018, *18* (15), 2225–2234.

(30) Sumer Gaaz, T.; Sulong, A. B.; Niaz Akhtar, M.; Amir, A.; Kadhum, H.; Bakar

Mohamad, A.; Al-Amiery, A. A.; Mcphee, D. J.; Kebangsaan Malaysia, U.; My, A. A. H. K. Properties and Applications of Polyvinyl Alcohol, Halloysite Nanotubes and Their Nanocomposites. 2015, *20* (12), 22833–22847.

(31)   Wang, M.; Yan, C.; M, L. Graphene Nanocomposites. In *Composites and Their Properties*; InTech, 2012, 17-36.

(32)   Hajeeassa, K. S.; Hussein, M. A.; Al-amshany, Z. M. The Influence of Graphene Nano-Particles on the Biological Interest of Polyvinyl Alcohol Nanocomposites. 2017, 3(1), 230-232

(33)   Suk, J. W.; Piner, R. D.; An, J.; Ruoff, R. S. Mechanical Properties of Monolayer Graphene Oxide. 2010, *4* (11), 6557–6564.

(34)   Qin, Z.; Taylor, M.; Hwang, M.; Bertoldi, K.; Buehler, M. J. Effect of Wrinkles on the Surface Area of Graphene: Toward the Design of Nanoelectronics. 2014, *14*(11), pp.6520-6525.

(35)   Akinwande, D.; Brennan, C. J.; Bunch, J. S.; Egberts, P.; Felts, J. R.; Gao, H.; Huang, R.; Kim, J.-S.; Li, T.; Li, Y.; et al. A Review on Mechanics and Mechanical Properties of 2D Materials—Graphene and Beyond. *Extrem. Mech. Lett.* 2017, *13*, 42–77.

(36)   Bozdoğan, A.; Aksakal, B.; Şahintürk, U.; Yargı, Ö. Influence of Heating on Spectroscopic, Mechanical, and Thermal Properties of Reduced Graphene Oxide-Poly(Vinyl Alcohol) Composite Films. *J. Mol. Struct.* 2018, *1174*, 133–141.

(37)   4 – Fundamental Properties of Graphene. In *Graphene*; 2018; pp 73–102.

(38)   Montes-Navajas, P.; Asenjo, N. G.; Santamaría, R.; Menéndez, R.; Corma, A.; García, H. Surface Area Measurement of Graphene Oxide in Aqueous Solutions. *Langmuir* 2013, *29* (44), 13443–13448.

(39)   Marinho, B.; Ghislandi, M.; Tkalya, E.; Koning, C. E.; de With, G. Electrical Conductivity of Compacts of Graphene, Multi-Wall Carbon Nanotubes, Carbon Black, and Graphite Powder. *Powder Technol.* 2012, *221*, 351–358.

(40)   Wang Z. Progress on preparation of graphene and its application. InIOP

Conference Series: Materials Science and Engineering 2017 Sep (Vol. 242, No. 1, p. 012032). IOP Publishing.

(41)   Cheun Lee, H.; Liu, W.-W.; Chai, S.-P.; Rahman Mohamed, A.; Aziz, A.; Khe, C.-S.; S Hidayah, N. M.; Hashim, U. Review of the Synthesis, Transfer, Characterization and Growth Mechanisms of Single and Multilayer Graphene. **2017,** *7*(26), 15644-15693.

(42)   Güler, Ö.; Güler, S. H.; Selen, V.; Albayrak, M. G.; Evin, E. Production of Graphene Layer by Liquid-Phase Exfoliation with Low Sonication Power and Sonication Time from Synthesized Expanded Graphite. *Fullerenes, Nanotub. Carbon Nanostructures* 2016, *24* (2), 123–127.

(43)   Krane N. Preparation of Graphene Selected Topics in Physics: Physics of Nanoscale Carbon. Growth Lakel. 1993;4:1-5.

(44)   Bhuyan, M. S. A.; Uddin, M. N.; Islam, M. M.; Bipasha, F. A.; Hossain, S. S. Synthesis of Graphene. *Int. Nano Lett.* 2016, *6* (2), 65–83.

(45)   Kelly, K. F.; Billups, W. E. Synthesis of Soluble Graphite and Graphene. *Acc. Chem. Res.* 2013, *46* (1), 4–13.

(46)   Saravanan, N.; Rajasekar, R.; Mahalakshmi, S.; Sathishkumar, T. P.; Sasikumar, K.; Sahoo, S. Graphene and Modified Graphene-Based Polymer Nanocomposites-A Review. 2013.

(47)   Yousefi, N.; Sun, X.; Lin, X.; Shen, X.; Jia, J.; Zhang, B.; Tang, B.; Chan, M.; Kim, J.-K. Highly Aligned Graphene/Polymer Nanocomposites with Excellent Dielectric Properties for High-Performance Electromagnetic Interference Shielding. *Adv. Mater.* 2014, *26* (31), 5480–5487.

(48)   Md Arephin Al Islam1, A. F. M. Mustafizur Rahman1, Sazia Iftekhar1, Khandoker Samaher Salem1, Nahida Sultana1, M. L. B. Morphology, Thermal Stability, Electrical, and Mechanical Properties of Graphene Incorporated Poly(Vinyl Alcohol)-Gelatin Nanocomposites. *Int. J. Compos. Mater.* 2016, *6* (6), 172–182.

(49)   Das, S.; Irin, F.; Tanvir Ahmed, H. S.; Cortinas, A. B.; Wajid, A. S.; Parviz, D.;

Jankowski, A. F.; Kato, M.; Green, M. J. Non-Covalent Functionalization of Pristine Few-Layer Graphene Using Triphenylene Derivatives for Conductive Poly (Vinyl Alcohol) Composites. *Polymer (Guildf).* 2012, *53* (12), 2485–2494.

(50) Ma, Y.; Bai, D.; Hu, X.; Ren, N.; Gao, W.; Chen, S.; Chen, H.; Lu, Y.; Li, J.; Bai, Y. Robust and Antibacterial Polymer/Mechanically Exfoliated Graphene Nanocomposite Fibers for Biomedical Applications. *ACS Appl. Mater. Interfaces* 2018, *10* (3), 3002–3010.

(51) Ghobadi, S.; Sadighikia, S.; Papila, M.; Fevzi, A.; Cebeci, Ç.; Alkan, S. Graphene-Reinforced Poly(Vinyl Alcohol) Electrospun Fibers as Building Blocks for High Performance Nanocomposites. 2015.

(52) Li, Y.; Umer, R.; Samad, Y. A.; Zheng, L.; Liao, K. The Effect of the Ultrasonication Pre-Treatment of Graphene Oxide (GO) on the Mechanical Properties of GO/Polyvinyl Alcohol Composites. *Carbon N. Y.* 2013, *55*, 321–327.

(53) Huang, Y.; Zhang, M.; Ruan, W. High-Water-Content Graphene Oxide/Polyvinyl Alcohol Hydrogel with Excellent Mechanical Properties †. 2014.

(54) Kang, D.; Shin, Y.-E.; Jo, H. J.; Ko, H.; Shin, H. S. Mechanical Properties of Poly(Dopamine)-Coated Graphene Oxide and Poly(Vinyl Alcohol) Composite Fibers Coated with Reduced Graphene Oxide and Their Use for Piezoresistive Sensing. *Part. Part. Syst. Charact.* 2017, *34* (9), 1600382.

(55) Liang, J.; Huang, Y.; Zhang, L.; Wang, Y.; Ma, Y.; Guo, T.; Chen, Y. Molecular-Level Dispersion of Graphene into Poly(Vinyl Alcohol) and Effective Reinforcement of Their Nanocomposites. *Adv. Funct. Mater.* 2009, *19* (14), 2297–2302.

(56) Guo, J.; Ren, L.; Wang, R.; Zhang, C.; Yang, Y.; Liu, T. Water Dispersible Graphene Noncovalently Functionalized with Tryptophan and Its Poly(Vinyl Alcohol) Nanocomposite. *Compos. Part B Eng.* 201**1**, *42* (8), 2130–2135.

(57) Ma, H.-L.; Zhang, Y.; Hu, Q.-H.; He, S.; Li, X.; Zhai, M.; Yu, Z.-Z. Enhanced Mechanical Properties of Poly(Vinyl Alcohol) Nanocomposites with Glucose-Reduced Graphene Oxide. *Mater. Lett.* 2013, *102–103*, 15–18.

(58) Mo, S.; Peng, L.; Yuan, C.; Zhao, C.; Tang, W.; Ma, C.; Shen, J.; Yang, W.; Yu, Y.; Min, Y.; et al. Enhanced Properties of Poly(Vinyl Alcohol) Composite Films with Functionalized Graphene. 2015.

(59) Yu, D. S.; Kuila, T.; Kim, N. H.; Lee, J. H. Enhanced Properties of Aryl Diazonium Salt-Functionalized Graphene/Poly(Vinyl Alcohol) Composites. *Chem. Eng. J.* 2014, *245*, 311–322.

(60) Johnson, D. W.; Dobson, B. P.; Coleman, K. S. A Manufacturing Perspective on Graphene Dispersions. *Curr. Opin. Colloid Interface Sci.* 2015, *20* (5–6), 367–382.

(61) Müller, K.; Bugnicourt, E.; Latorre, M.; Jorda, M.; Echegoyen Sanz, Y.; Lagaron, J. M.; Miesbauer, O.; Bianchin, A.; Hankin, S.; Bölz, U.; et al. Review on the Processing and Properties of Polymer Nanocomposites and Nanocoatings and Their Applications in the Packaging, Automotive and Solar Energy Fields. *Nanomaterials* 2017, *7*, 74.

(62) Schadler, L. S.; Brinson, L. C.; Sawyer, W. G. *Overview Nanocomposite Materials Polymer Nanocomposites: A Small Part of the Story**; 2007.

(63) Tang, L.-C.; Zhao, L.; Guan, L.-Z. 7 Graphene/Polymer Composite Materials: Processing, Properties and Applications. *Adv. Compos. Mater. Prop. Appl.* 2017, 349–419.

(64) Puggal, S.; Dhall, N.; Singh, N.; Litt, M. S. A Review on Polymer Nanocomposites: Synthesis, Characterization and Mechanical Properties. *Indian J. Sci. Technol. 9* (4), 10.

(65) Song, K. CUSTOMIZING FIBER SPINNING APPROACHES FOR POLYMER/NANO-CARBON COMPOSITES, Northeastern University Boston, Massachusetts, 2014.

(66) Puchý1, V.; Tatarko1, P.; Dusza1, J.; Morgiel2, J.; Bastl3, Z.; Mihály4, J.; Kaushik, P. *Characterization of Carbon Nanofibers by SEM, TEM, ESCA and Raman Spectroscopy*.

(67) Joshi, M.; Bhattacharyya, A.; Wazed Ali, S. *Characterization Techniques for*

Nanotechnology Applications in Textiles; 2008; Vol. 33.

(68) Speakman, S. A. *Basics of X-Ray Powder Diffraction Training to Become an Independent User of the X-Ray SEF at the Center for Materials Science and Engineering at MIT*.

(69) Murthy, N. S. Experimental Techniques for Understanding Polymer Crystallization. *Cryst. Multiph. Polym. Syst.* 2018, 49–72.

(70) Speakman, S. A. *Estimating Crystallite Size Using XRD Using XRD Using XRD Using XRD*.

(71) Johnson, D. W.; Dobson, B. P.; Coleman, K. S. A Manufacturing Perspective on Graphene Dispersions. *Curr. Opin. Colloid Interface Sci.* 2015, *20* (5–6), 367–382.

(72) Paredes, J. I.; Villar-Rodil, S.; Martínez-Alonso, A.; Tascón, J. M. D. Graphene Oxide Dispersions in Organic Solvents.

(73) Rodgers, A. N. J.; Velický, V.; Dryfe, R. A. W. Electrostatic Stabilization of Graphene in Organic Dispersions. 2015.

(74) Gupta, D.; Jassal, M.; Agrawal, A. K. The Electrospinning Behavior of Poly(Vinyl Alcohol) in DMSO-Water Binary Solvent Mixtures. 2016, *6*, 102947–102955.

(75) Kuo, C. J.; Lan, W. L. Gel Spinning of Synthetic Polymer Fibres. *Adv. Filam. Yarn Spinn. Text. Polym.* 2014, 100–112.

(76) ZhanpingYANG, by; Zhang, L.; Chen, R.-X.; Cao, J.-H.; Liu, F.-J. Optimal Spinneret Size for Improvement of Fibers Mechanical Property THERMAL SCIENCE. 2013, *17* (5), 1501–1503.